TITLE
KRAS-mediated upregulation of CIP2A promotes suppression of PP2A-B56α to initiate pancreatic cancer development.

AUTHORS AND AFFILIATIONS
Samantha L. Tinsley[1,2], Rebecca A. Shelley[2], Gaganpreet K. Mall[2], Ella Rose D. Chianis[2], Alisha Dhiman[6], Garima Baral[2], Harish Kothandaraman[6], Mary C. Thoma[3], Colin Daniel[3], Nadia Atallah Lanman[5], Marina Pasca di Magliano[4], Goutham Narla[4], Luis Solorio[1,7], Emily C. Dykhuizen[1,6], Rosalie C. Sears[3], Brittany L. Allen-Petersen[1,2,8]*

[1]Purdue University Interdisciplinary Life Sciences Program (PULSe), Purdue University, West Lafayette, IN, USA
[2]Department of Biological Sciences, Purdue University, West Lafayette, IN USA
[3]Department of Molecular Medicine and Genetics, Oregon Health and Sciences University, Portland, Oregon, USA
[4]University of Michigan School of Medicine, University of Michigan, Ann Arbor, Michigan, USA
[5]Collaborative Core for Cancer Bioinformatics, Purdue University, West Lafayette, IN, USA
[6]Department of Medicinal Chemistry and Molecular Pharmacology, Purdue University, West Lafayette, IN, USA
[7]Department of Biomedical Engineering, Purdue University, West Lafayette, IN, USA
[8]Purdue Institute for Cancer Research, Purdue University, West Lafayette, IN, USA

RUNNING TITLE
PP2A-B56α suppression promotes pancreatic cancer initiation

KEYWORDS
PP2A, CIP2A, KRAS, PDAC, ADM

***Corresponding Author**
Brittany L. Allen-Petersen, Purdue University, 201 S. University St., West Lafayette, IN 47907.
Phone: 765-496-1896 Email: ballenpe@purdue.edu

ABSTRACT

Oncogenic mutations in KRAS are present in approximately 95% of patients diagnosed with pancreatic ductal adenocarcinoma (PDAC) and are considered the initiating event during the development of pancreatic intraepithelial neoplasia (PanIN) precursor lesions. While it is well established that KRAS mutations can drive the initiation of pancreatic oncogenesis, the effects of oncogenic KRAS signaling on regulation of phosphatases during this process is not fully appreciated. Protein Phosphatase 2A (PP2A) has been implicated in suppressing KRAS-driven cellular transformation. However, low PP2A activity is observed in PDAC cells compared to non-transformed cells, suggesting that suppression of PP2A activity is an important step in the

overall development of PDAC. In the current study, we demonstrate that $KRAS^{G12D}$ induces the expression of both Cancerous Inhibitor of PP2A (CIP2A), an endogenous inhibitor of PP2A activity, and the PP2A target, c-MYC. Consistent with these findings, $KRAS^{G12D}$ sequestered the specific PP2A subunit responsible for c-MYC degradation, B56α, away from the active PP2A holoenzyme in a CIP2A-dependent manner. During PDAC initiation *in vivo*, knockout of B56α promoted $KRAS^{G12D}$ tumorigenesis by accelerating acinar-to-ductal metaplasia (ADM) and the formation of PanIN lesions. The process of ADM was attenuated *ex vivo* in response to pharmacological re-activation of PP2A utilizing direct small molecule activators of PP2A (SMAPs). Together, our results suggest that suppression of PP2A-B56α through KRAS signaling can promote Myc-driven initiation of pancreatic tumorigenesis.

INTRODUCTION

Development of mutations in protooncogene Kirsten Rat Sarcoma viral oncogene homolog (KRAS) is known to be a driver of many common cancers, such as lung cancer, colorectal cancer, and pancreatic cancer (1). Pancreatic ductal adenocarcinoma (PDAC) has the lowest five-year survival rate (12%) of all major cancers(2). Within PDAC tumors, oncogenic KRAS mutations occur in approximately 95% of all patients, underscoring the importance of this signaling pathway to patient outcomes (3). Data generated from genetic mouse models have established that expression of mutant KRAS in the pancreas drives the initiation of pancreatic cancer and helps to maintain malignant tumor growth (4,5). Acinar-to-ductal metaplasia (ADM) is a reversable process by which pancreatic acinar cells undergo a transdifferentiation process to a duct-like state in response to exogenous stressors, such as wound infliction or inflammation(6). However, in the presence of oncogenic KRAS, this process becomes permanent and leads to the formation of pancreatic intraepithelial neoplasia (PanIN) precursor lesions (6). Historically, KRAS mutations alone have not been sufficient to transform normal cells to malignant cells and often causes oncogene-induced senescence (4,7). However,

inhibition of Protein Phosphatase 2A (PP2A) combined with oncogenic KRAS mutations is adequate for malignant transformation, implicating PP2A as a critical regulator of KRAS signaling (8).

PP2A is a heterotrimeric holoenzyme composed of three individual subunits that allow for almost 90 unique complexes: the (A) scaffolding subunit, the (B) substrate specificity regulatory subunit, and the (C) catalytic subunit (9). The B subunits are broken down into four main families: B (B55), B' (B56), B'', and B'''(Striatins). The impact of PP2A activity on oncogenic signaling heavily depends on which B subunit is incorporated into the complex and context in which it is studied. Using a targeted shRNA screen, Sablina et al. determined that loss of B56α could transform human embryonic kidney cells expressing $HRAS^{G12V}$, implicating the PP2A-B56α complex as a tumor suppressor. While the B56α subunit has been associated with the negative regulation of many KRAS signaling effectors, including MEK, ERK, and AKT and the oncoprotein c-MYC (MYC), the functional consequence of this subunit to PDAC tumor phenotypes is unknown (10–13). Therefore, understanding how oncogenic KRAS signaling and PP2A suppression intersect to promote initiation of pancreatic tumorigenesis is critical for a more complete insight into PDAC tumorigenesis and the development of new therapeutic strategies to target KRAS-mediated pathways.

Although loss of PP2A is associated with transformation, genetic deletion or non-functional mutation of PP2A subunits in cancer is extremely low (9). Conversely, we and others have determined that endogenous inhibitors of PP2A, such as Cancerous Inhibitor of PP2A (CIP2A), are commonly overexpressed in PDAC and contribute to tumor growth(14). In the current study, we demonstrate that induction of $KRAS^{G12D}$ in human pancreatic epithelial cells increases the expression of both CIP2A and the direct B56α target, MYC. This expression is associated with a decreased B56α incorporation into the PP2A holoenzyme and is rescued with the loss of CIP2A. To determine the functional consequence of B56α *in vivo*, we crossed our

B56α hypomorphic mouse (B56α$^{hm/hm}$)(15) with oncogenic KRAS^{G12D} in the pancreas. Loss of B56α significantly accelerated KRAS^{G12D}-driven ADM and PanIN formation. Finally, treatment of ADM cultures *ex vivo* with the small molecule activator of PP2A, DT061, prevented the transdifferentiation of ductal-like cells. Together, these findings implicate the inhibition of PP2A-B56α as a critical early event in PDAC initiation and highlight the understudied potential of protein phosphatases as actionable therapeutic targets.

RESULTS

Induction of KRAS^{G12D} promotes CIP2A-mediated suppression of PP2A-B56α in pancreatic epithelial cells.

Previous studies have suggested that CIP2A and KRAS may function synergistically and display a significant overlap in downstream regulated pathways, suggesting that these two pathways may intersect (16–18). To determine the acute effects of oncogenic KRAS on CIP2A expression, a non-transformed human pancreatic ductal epithelial cell line (HPDE) with tet-inducible KRAS^{G12D} (HPDE-iKRAS) was treated with 50ng/mL doxycycline (dox) in a timecourse from 0-12hr. This system allows for the potent induction of KRAS^{G12D} (**Fig S1A**) and activation of the downstream Mitogen-activated protein kinase (MAPK) pathway, with peak phospho-ERK (pERK, p-p42/44) levels seen at 8hrs post-dox treatment. KRAS^{G12D} induction resulted in a time-dependent increase in CIP2A expression, with significant upregulation seen by 8-12hr (**Fig 1A, B, D**). PP2A-B56α provides critical posttranslational regulation of MYC by dephosphorylating MYC at serine62 (pS62 Myc) and driving MYC proteasomal degradation (19,20). Consistent with increased expression of CIP2A and PP2A inhibition, KRAS^{G12D} induction significantly increased MYC protein (**Fig 1A, C**) in a manner that mirrored CIP2A kinetics. In contrast, there was no change in *MYC* mRNA levels (**Fig S1A**), supporting a posttranslational regulatory event.

To identify the impact of KRAS^{G12D} on the ability of cells to form an active PP2A-B56α holoenzyme, HPDE-iKRAS cells were treated with dox for 8 hrs and the interaction between the

catalytic subunit of PP2A (PP2Ac) and B56α was determined using a proximity ligation assay (PLA). Consistent with the functional inhibition of PP2A-B56α, dox treatment significantly reduced the association of B56α with PP2Ac (**Fig 1E-F**). This reduction was dependent on CIP2A as knockdown of CIP2A with siRNA (siCIP2A) significantly increased the number of PP2Ac-B56α complexes in -dox conditions and prevented the $KRAS^{G12D}$-induced loss of PP2Ac-B56α association in +dox conditions (**Figure 1E-F, S1B**). Consistent with the retained association of PP2A-B56α, transient knock down of CIP2A (siCIP2A) reduced clonogenic colony growth in HPDE-iKRAS cells non-targeting siRNA (siNT) treated cells (**Fig S1C-D**).

To identify whether $KRAS^{G12D}$ expression correlates with lower PP2A function during pancreatic cancer disease progression, we utilized a *PDX1-Cre; LSL-KRAS^{G12D}* (KC) mouse model and stained pancreatic tissue at 1-, 2-, and 5-months of age for CIP2A (PP2A inhibitor) and pS62 MYC (PP2A target), and pan-Cytokeratin (epithelial populations) (**Fig 1G**). Compared to normal pancreata from WT mice, there was a significant increase in both CIP2A and pS62 MYC protein expression within precursor PanINs. Furthermore, this expression increased across time as PanINs progressed (**Fig 1G**). Together, these findings indicate that the functional inhibition of B56α downstream of $KRAS^{G12D}$ is an early event in PDAC development.

Loss of $KRAS^{G12D}$ alleviates CIP2A-mediated suppression of B56α

To identify whether $KRAS^{G12D}$ signaling is necessary to maintain CIP2A-mediated suppression of PP2A-B56α, we utilized a KRAS-addicted malignant cell line (iKRAS3) isolated from the tet-inducible $KRAS^{G12D}$ PDAC mouse model (iKRAS*) (5). In this system, cells are continuously cultured in dox-containing media and the removal of dox results in a loss of $KRAS^{G12D}$ expression. iKRAS3 cells were cultured with dox and then harvested 0, 24, 48, and 72 hours post-dox withdrawal. Consistent with dox-inducible $KRAS^{G12D}$ in Figure 1, pERK levels returned to baseline within 24 hrs after the loss of oncogenic $KRAS^{G12D}$ expression ($tKras^{G12D}$) (**Fig 2A-B**). Conversely, B56α levels increased by 24 hrs post-dox and remain elevated for the

rest of the timecourse. Inhibition of the MAPK pathway is known to attenuate MYC activity and stability (21). However, despite pERK levels being low, Myc levels remained high during the first 24 hrs, and then declined over time. The sustained Myc signaling at this timepoint correlates with a transient increase in CIP2A expression at 24 hrs that then rapidly dropped off, with a 60% inhibition of Myc occurring by 72 hrs (**Fig 2A-B**). While the loss of CIP2A at 72 hrs could be due to decreased transcription, *Myc* mRNA remained unchanged after 72 hrs (**Fig 2C**).

To determine if the loss of KRAS signaling promoting the loss of CIP2A and Myc protein expression is conserved *in vivo*, we utilized tissues from the iKRAS* mouse model with $KRAS^{G12D}$ induced for three weeks in the pancreas of adult mice and then pancreatic tissue harvested after one week of dox withdrawal (**Fig 2F**). Loss of $KRAS^{G12D}$ in this model leads to a dramatic remodeling of the pancreas, with decreased PanINs and a re-emergence of acinar tissue. Compared to dox conditions, loss of $KRAS^{G12D}$ significantly reduced both CIP2A and active Myc (pS62 Myc) protein expression. Together, these results demonstrate that KRAS drives and maintains CIP2A expression, suggesting that suppression of PP2A-B56α is likely important for initiating and promoting PDAC progression.

Overexpression of PP2A-B56α abrogates $KRAS^{G12D}$ tumorigenic phenotypes

Given that induction of KRAS signaling leads to the suppression of PP2A-B56α activation, we wanted to determine if genetic overexpression of the PP2A B56α subunit would be sufficient to abrogate oncogenic KRAS phenotypes. To test this, we overexpressed an HA-tagged B56α (HA-B56α) in malignant iKRAS3 cells (iKRAS3 B56αOE) and compared overall tumorigenic properties relative to empty vector controls (iKRAS3 EV) (22). First, we evaluated the effects of B56α overexpression on both anchorage-independent growth and self-renewal capabilities *in vitro* through soft agar (**Fig 3A-B**) and clonogenic assays (**Fig 3C-D**), respectively. We found that overexpression of PP2A-B56α abrogated both soft agar growth and

the clonogenic colony formation, indicating that PP2A-B56α expression is sufficient to antagonize oncogenic $KRAS^{G12D}$ signaling.

To test if B56α expression attenuates $KRAS^{G12D}$ *in vivo* tumor growth, iKRAS3 EV or B56αOE cell were orthotopically injected into the pancreas of *NOD.Cg-Rag1^{tm1Mom} Il2rg^{tm1Wjl}/SzJ* (NRG) mice and tumor growth was measured weekly by high-frequency ultrasound imaging. Overexpression of B56α significantly hindered *in vivo* tumor growth kinetics and resulted in a 50% reduction in tumor weight at endpoint (**Fig 3E-G**). Immunofluorescent staining of isolated tumor tissue in both the EV and B56αOE conditions shows that areas of HA-B56α expression correlated with lower levels of pS62 Myc (**Fig 3H**), demonstrating that increased B56α expression antagonizes Myc protein expression downstream of $KRAS^{G12D}$, leading to abrogated tumor growth.

Genetic loss of PP2A-B56α accelerates $KRAS^{G12D}$-driven acinar-to-ductal metaplasia *ex vivo*

Expression of $KRAS^{G12D}$ *in vivo* potently drives acinar-to-ductal metaplasia (ADM), the earliest step in PDAC progression (4). To understand how B56α expression contributes to the transdifferentiation process of ADM, we utilized genetic mouse models to perform *ex vivo* ADM assays(23). First, we isolated acinar cells from 5-6 week old WT, B56α hypomorph mice (B56α$^{hm/hm}$(15)), *PDX1-Cre; LSL-KRAS^{G12D}* (KC(4)), or *PDX1-Cre; LSL-KRAS^{G12D}; B56α$^{hm/hm}$* (KCB$^{hm/hm}$) mice and implanted the acinar clusters into a collagen matrix. The acinar clusters were imaged every six hours for three days to observe the kinetics of the acinar to ductal-like transdifferentiation. Analysis of the structures at 24, 48, and 72H revealed that loss of B56α significantly accelerated ADM, with more duct-like structures in the KCB$^{hm/hm}$ condition when compared to KC condition at 48H (**Fig 4A-B**). Further, kinetic quantification of cultures over time demonstrated that KCB$^{hm/hm}$ ductal-like structures emerge roughly 18 hrs prior to KC (**Fig 4C**) with significant upregulation seen at major time points (**Fig S2A)**. However, both KC and

KCB$^{hm/hm}$ conditions had completed the differentiation process after 72H of implantation in a collagen matrix.

To validate the transdifferentiation from an acinar identity to a ductal cell identity, cell were dissolved out of the collagen matrix at 24 and 48 hours and collected for RNA isolation to determine mRNA gene expression over time. Consistent with ductal differentiation, mRNA expression of the ductal marker, cytokeratin 19 (*Ck19)* (**Fig 4D**), and the ductal transcription factor, sry-box transcription factor 9 (*Sox9)*, (**Fig S2B**) show increased expression over time, with a significant upregulation in the KCB$^{hm/hm}$ condition by 48H. As structures differentiate from acinar to ductal, *Cip2a* mRNA is also upregulated suggesting the CIP2A-PP2A signaling axis is likely important in driving a ductal-like cell fate (**Fig S2D**). Additionally, *Myc* mRNA expression is also associated with ductal differentiation(24). Our data show that Myc mRNA is significantly upregulated between 24 and 48H in both the KC and KCB$^{hm/hm}$ conditions (**Fig S2C**).

To further validate large-scale changes in the transcriptionally driven process of ADM, we performed RNA-seq on the mRNA isolated from structures in the KC and KCB$^{hm/hm}$ conditions at 48H. Analysis of differentially regulated genes (DEGs) resulted in 356 genes upregulated and 72 genes downregulated (FDR<0.05) in KCB$^{hm/hm}$ structures when compared to KC structures (**Fig 4E**). Gene set enrichment analysis of DEGs ranked by expression levels indicate that with the loss of B56α expression, KRAS signaling is significantly upregulated (**Fig 4F**). This increase is consistent with B56α overexpression antagonizing KRAS^{G12D} phenotypes in Figure 3. Additionally, the transdifferentiation signature of epithelial-to-mesenchymal transition (EMT) is also upregulated when compared to KC structures, suggesting that loss of B56α may increase cellular plasticity and the ability to undergo ADM (**Fig 4G**).

Loss of PP2A-B56α accelerates KRAS^{G12D} PDAC initiation *in vivo*

The pancreas-specific expression of KRAS^{G12D} faithfully recapitulates pancreatic cancer initiation, including ADM and the formation of PanINs *in vivo* (4,5). This progression is marked

by a loss of acinar tissue, formation of mucin producing PanIN lesions, and stromal expansion. To determine if the loss of B56α can promote PDAC initiation *in vivo*, pancreata from WT, B56α$^{hm/hm}$, KC, and KCB$^{hm/hm}$ were harvested at 2-month and 5-month timepoints and evaluated for changes associated with early PDAC progression. B56α$^{hm/hm}$ mice display normal pancreatic histology, indicating that the loss of B56α alone is not sufficient to drive PDAC initiation. However, consistent with our *in vitro* ADM findings (**Fig 4**), there was a reduction in healthy acinar area starting at 2 months of age in KCB$^{hm/hm}$ mice compared to KC mice, with a significant loss by 5 months (**Fig 5A-B**). We then stained pancreatic tissues with alcian blue, a basic dye that positively labels acidic patches of mucin expression within PanIN lesions, to determine the impact on progression. Loss of B56α resulted in accelerated PanIN formation, with KCB$^{hm/hm}$ mice displaying a significant increase in alcian blue positive lesions at both 2 and 5 months of age compared to KC tissues (**Fig 5A, D**). These aberrant morphological changes within KCB$^{hm/hm}$ tissues were accompanied by increased collagen deposition, a hallmark of PDAC progression (25), as indicated by masson's trichrome (MTC) (**Fig 5A, C**). Together, the decrease in healthy acinar area, increase in PanIN lesions, and increase in collagen deposition suggest that loss of B56α cooperates with KRAS^{G12D} to accelerate PDAC initiation and the development of pre-malignant lesions.

Based on our findings that KRAS^{G12D} increases the expression of CIP2A and reduces B56α activity (**Figure 1, 2**), we analyzed Cip2a and Myc expression within acinar and ductal populations (**Fig 5F-G, Fig S3A-B**). Cip2a expression was strongly correlated with PanCK+ cells in both KC and KCB$^{hm/hm}$, alluding to a role of PP2A-suppression in promoting the ductal identity. Low level expression of pS62 Myc was observed in both acinar and ductal populations of 2-month KC tissues, which increased in PanIN lesions by 5 months (**Fig 5E-F, S3A-B**). In contrast, the loss of B56α increased pS62 Myc in both of these populations in 2- and 5-month KCB$^{hm/hm}$ tissues. Overall, these results suggest that PP2A-B56 α plays an important role in

restraining pancreatic cellular plasticity during PDAC initiation and the suppression of this subunit significantly contributes to oncogenic KRAS PDAC progression.

Therapeutic Reactivation of PP2A-B56α promotes attenuates process of ductal transdifferentiation

Since the active PP2A holoenzyme requires the association of three individual subunits (A, B, and C), genetic strategies to model B56α activation are limited. Therefore, to determine if pharmacological activation of PP2A can prevent acinar cells from undergoing ADM, we took advantage of the small molecule activator of PP2A (SMAP), DT061. This compound binds at the interface of all three PP2A subunits (A, B, and C) and functions to nucleate the PP2A holoenzyme (26). While DT061 broadly activates PP2A, it has been shown that it preferentially promotes the stabilization of B56α into the PP2A complex compared to other B subunits. Acinar cells isolated from KC pancreata were plated in an ADM assay and treated with either DMSO control or increasing doses of DT061 for 72H (**Fig 6A**). Endpoint cultures were then quantified for acinar or ductal-like structures. Our data show that DT061 reduced the percent of duct-like structures in a dose-dependent fashion (**Fig 6B**), and the ductal structures that did form were significantly smaller compared to control (**Fig 6C, D**). To validate that the phenotypic loss of ductal-like cells correlates with a loss of ductal identity, we isolated RNA from the endpoint structures in each condition and ran qPCR for ductal identity markers. We found that increasing doses of DT061 led to lower levels of canonical ductal markers, *Ck19* and *Sox9* (**Fig 6E, F**). DT061 also decreased mRNA levels of *Cip2a* and *Myc* (**Fig 6G, H**) and increased B56α (*Ppp2r5a*) (**Fig 6I**), consistent PP2A activation antagonizing ductal differentiation.

Recent studies have demonstrated that inhibition of mutant KRAS with the small molecule, MRTX1133, results in strong tumor suppression in KPC allografts(27). As $KRAS^{G12D}$ inhibited PP2A function and increased oncogenic MYC levels, (**Figures 1**) and activation of PP2A with DT061 attenuated $KRAS^{G12D}$ phenotypes, we wanted to investigate whether DT061

could suppress late-stage PDAC tumor growth. For these studies, we monitored KPC (*LSL-KRAS$^{G12D/+}$; P53$^{-/+}$; PDX1-Cre)* mice weekly by high-frequency ultrasound, and then randomly enrolled mice into treatment arms when tumors reached 5-7mm in diameter. This highly aggressive genetic mouse model accurately reproduces several aspects of human PDAC disease, including desmoplasia and metastatic disease, and is therapeutically refractory to most standard-of-care chemotherapies(28). Consistent with the ability of B56α overexpression to suppress iKRAS3 tumors (**Figure 3**), DT061 significantly increased the overall survival of KPC mice compared to vehicle treated animals (**Fig 6J**). Together, these results suggest that therapeutic re-activation of PP2A can antagonize both the initiation and the progression of PDAC tumors *in vivo*.

DISCUSSION

In this study, we have determined a mechanism by which oncogenic KRAS signaling inhibits PP2A-B56α activity to promote initiation of pancreatic cancer. Our data show that KRAS signaling promotes the upregulation of the PP2A-B56-specific endogenous inhibitor, CIP2A, which sequesters B56α out of the PP2A complex. We also find that PP2A-B56α negatively regulates the progression of acinar-to-ductal metaplasia and initiation of pancreatic precursor lesions, as loss of B56α accelerates the progression of these phenotypes. Previous studies demonstrate that transcriptional deregulation of MYC can accelerate KRAS^{G12D} PDAC tumor development and is necessary to maintain tumor growth (24). However, MYC is known to be tightly regulated at the transcriptional, translational, and posttranslational levels. We find that the inhibition of B56α increased expression of the active form of MYC (pS62) during PDAC progression, implicating the posttranslational regulation of MYC as critical mechanism of PDAC tumor suppression. These findings also indicate that the contribution of aberrant MYC signaling in the absence of transcriptional alterations may be grossly underestimated in PDAC patients.

Previous studies have implicated upregulation of CIP2A expression through RAS-mediated signaling networks including HER-family and MAPK signaling (29). Translational regulation of CIP2A through transcription factor, ETS1, is also driven through increased MAPK signaling (30). Our studies support the notion that CIP2A transcription and translation are regulated through the activation of KRAS and the MAPK pathway. This mechanism further promotes oncogenesis through PP2A-B56 inhibition by CIP2A, however how KRAS signaling drives and maintains expression of CIP2A in PDAC remains to be explored.

Using *ex vivo* implantation of acinar clusters to measure ADM, we demonstrated that the acceleration of transdifferentiation by loss of B56α is a cell intrinsic process. As the process of ADM is transcriptionally mediated, accelerated transdifferentiation may be due to changes in overall epigenetic regulation. This is consistent with the recently published data that RAS signaling and loss of PP2A signaling changes converge at co-regulation of epigenetic modifiers (31). Overall, our understanding of the posttranslational regulation of epigenetics by PP2A is still in its infancy. Therefore, further insight into how B56α alters epigenetic regulation of the ADM is of critical importance.

PP2A is a unique tumor suppressor as it is rarely genetically deleted or mutated. Instead, loss of PP2A activity is primarily driven through suppression by endogenous inhibitors like CIP2A(9). Since the ability of PP2A to form a functional holoenzyme remains intact, the therapeutic re-activation of this phosphatase has shown strong preclinical responses in several cancers, including prostate, ovarian, breast and lung cancers (32–36). Furthermore, activation of PP2A, either through genetic or pharmacological means, functions synergistically with various kinase inhibitors implicating PP2A as a critical rheostat of therapeutic response (16,31,37). Our studies show that DT061 not only abrogates the process of ADM, but also improves long-term survival of spontaneously driven PDAC in KPC mice when treated with DT061. Since DT061 preferentially incorporates B56α into the PP2A holoenzyme these results strongly support a

critical role for this subunit in *in vivo* tumor progression and support further investigation into the mechanisms by which therapeutic re-activation of PP2A regulates late-stage disease (26). Given that each PP2A B subunit potentially has unique and context dependent functions, the development of therapeutic compounds that leverage individual subunits would be an extremely impactful clinical advancement.

Finally, our studies represent one of the few *in vivo* experimental models of PP2A B subunits. Redundancy between PP2A subunits has been a confounding factor in the field and potentially mask the contribution of specific PP2A complexes, like PP2A-B56α, to tumor function. It is unknown if loss of one B subunit drives the incorporation of another into the PP2A complex. Therefore, it is essential that future studies analyze the dynamic interactions between B subunits within tumors.

In summary, our *in vitro* and *in vivo* results implicate the inhibition of PP2A-B56α downstream of oncogenic KRAS as a key step in promoting cellular plasticity and the initiation of pancreatic cancer.

METHODS

Cell Culture

iKRAS #3 cells were cultured in RPMI1640 + 10% fetal bovine serum. iKRAS #3 cells were maintained in 1ug/mL doxycycline (dox). HPDE-iKRAS cells were cultured in Keratinocyte Serum-Free Media (KSFM) supplemented with epidermal growth factor and bovine pituitary extract (Fisher Scientific #17-005-042). Virus to construct stable HA-B56a overexpression cell lines were produced using HEK293T cells transfected using Lipofectamine 3000 (Fisher Scientific, #L3000015) with the plasmid of interest (POI) and two plasmids encoding packaging proteins for viral vector (pAX.2, pMD2.G). Media containing viral particles harvested and stored at -80°C until use. Parental cells were treated with 10ug/mL polybrene for 1 hour before adding

viral particles to media. Media was changed after 24H and selected using antibiotic matching POI. Concentration for antibiotic for selection of stable cell lines were determined using a kill curve and cells were treated with minimum amount of antibiotic needed to kill all parental cells. Cells transfected with siCIP2A (Horizon Discovery, #L-014135-01-0005) were transiently transfected using Lipofectamine and then utilized 24-72H after transfection.

Quantitative RT-PCR

RNA was isolated using the ThermoScientific GeneJET Purification Kit (Thermofisher, #K0732). Eluted RNA concentration was measured using the Synergy H1. Reverse transcription PCR was performed using the High Capacity cRNA Reverse Transcription Kit (Fisher Scientific, #43-688-14) and the following PCR procedure: 25°C 10 minutes, 37°C 120 minutes, 85°C 5 minutes, HOLD at 4°C. Quantitative PCR is performed on the QuantStudio 3 using SYBR Green (Fisher Scientific, #A25743) and the primers listed on the table below made custom from Integrated DNA Technologies.

Gene Name	Species	Forward Sequence	Reverse Sequence
B56a	*Mouse*	5'-ATTAAAAgAgCgACgCTgAATgA-3'	3'-TCTTCCgggTCAAAATCTggAT-5'
CIP2A	*Mouse*	5'-gCTTgCCACAATgATTCCgTg-3'	3'-gCCAATAgTCCTAgACAAggCAT-5'
Myc	*Mouse*	5'-CCTAgTgCTgCATgAggAgAC-3'	3'-CCTCATCTTCTTgCTCTTCTTCA-5'
Sox9	*Mouse*	5'-AgTACCCgCATCTgCACAAC-3'	3'-ACgAAgggTCTCTTCTCgCT-5'
tKRAS	*Mouse*	5'-CAAggACAAggTgTACAgTTATgTgACT-3'	3'-gCCTgCgACggCggCATCTgC-5'
KRAS	*Mouse*	5'-CgCggAATTCggCCTgCTgAAAATgACTgAg-3'	3'-gACAggATCCTCACATAACTgTACACCTTgTCC-5'
CK19	*Mouse*	5'-gACCTAgCCAAgATCCTgAgT-3'	3'-TCAgCTCCTCAATCCgAgCA-5'
GAPDH	*Mouse*	5'-CgTCCCgTAgACAAAATggT-3'	3'-TTgATggCAACAATCTCCAC-5'
B56a	*Human*	5'-AgAgCCCTgATTTCCAgCCTA-3'	3'-TTTCCCATAAATTCggTgCAgA-5'
CIP2A	*Human*	5'-gCCACACTgATTCggTgTTTT-3'	3'-TgCCgACAAAgATTTgCCAATA-5'

Myc	*Human*	5'-CAAACCTCCTCACAgCCCACT-3'	3'-TTCgCCTCTTgACATTCTCCTC-5'
KRAS	*Human*	5'-TggTAgTTggAgCTggTggCg-3'	3'-TCCTCTTgACCTgCTgTgTCg-5'
TBP	*Human*	5'-TgCACAggAgCCAAgAgTgAA-3'	3'-CACATCACAgCTCCCCACCA-5'

Western Blot Analysis

Changes in protein signaling were assessed using a western blotting technique. First, the cells were lysed in an AB lysis buffer (20mM Tris pH7.5, 50mM NaCl, 0.5% Triton X-100, 0.5% deoxycholate, 0.5% SDS, and 1mM EDTA). Proteins scraped off plate using cell scraper and then passed through an insulin needle to ensure proper lysis. Cells were incubated on ice for 15-60min, vortexing periodically. Protein concentration was then measured using the DC protein assay kit (Bio-Rad, #5000112) and absorbance was read on the Synergy H1. Using a BSA standard curve, the protein concentration was calculated. Lysate was then treated with SDS sample buffer (57.5% glycerol, 125mM Tris pH 6.8, 5% SDS, 5% b-mercaptoethanol, bromophenol blue) and boiled at 95°C for 5 minutes. SDS page was run on 4-15% gradient protein gels using the Criterion Electrophoresis Cell (Bio-Rad, #1656001) and transferred to a PVDF membrane using the Trans-Blot semi-dry transfer system (Bio-Rad, #1704150). Membrane was blocked in Licor TBS blocking buffer (Fisher Scientific, #NC1660550) for 1H at RT and then incubated with primary antibody overnight at 4°C. Membranes were then washed 3x5 minutes in 1XTBST (0.1% tween-20), incubated with secondary antibody for 1H at RT, then washed again 3x5 minutes with 1XTBST. Membranes were then scanned using the Licor Odyssey DLx Imaging system and analyzed using Image Studio software.

Gene Name	Catalog Number	LOT Number	Company
KIAA1524	HPA039570	000008181	Atlas Biosciences
CIP2A	sc-80659	H2522	Santa Cruz Biotechnologies
B56a	C Terminal Clone 3A6D3	N/A	Egon Ogris Lab
Myc	ab32072	GR3377350-8-YR091119PS	Abcam

GAPDH	M4300	820845	ThermoFisher
Phospho-ERK 1/2 (pS42, pS44)	9101	31	Cell Signaling Technologies
ERK 1/2	4695	28	Cell Signaling Technologies
IRDye 680RD Goat anti-Rabbit	926-68071	D20809-05	Licor
IRDye 800CW Goat anti-Mouse	926-32210	D20802-25	Licor

Proximity Ligase Assay

The Duolink In Situ Red Starter Kit (Millipore Sigma, #DUO92101) following protocol provided by Millipore Sigma with an extended amplification period of 3H instead of the recommended 1H. Treated cells were then counterstained with DAPI for 5 minutes and ActinGreen 488 (Thermofisher, #R37110) for 20 minutes at RT. Cells were imaged using the Nikon Eclipse N_i upright fluorescent microscope. Fluorescent images were gated in FIJI and PLA puncta per cell were quantified and analyzed using a one-way ANOVA.

Soft Agar Assay

To perform this assay, a 12 well plate was coated 500uL with a 1:1 mixture of 1.4% noble agar solution mixed and 2X RPMI media supplemented with 20% FBS. Then 40,000 cells/well were resuspended in 2X RPMI+20% FBS media and mixed 1:1 with a 0.7% noble agar solution. 500uL of the cell suspension was plated per well and allowed to solidify at RT. Finally, the cells were topped with 1mL 1XRPMI +10% FBS per well and treated with a final concentration of 1ug/mL dox. Cells were allowed to grow for two weeks and dox was re-dosed every 3-4 days. Colonies were measured by percent area covered using FIJI and conditions were statistically analyzed using a student's t-test between conditions.

Clonogenic Assay

One thousand cells were seeded per well in a 6-well plate. HPDE-iKRAS cells were supplemented with 50ng/mL doxycycline every 48-72H. Cells were allowed to grow for six to seven days and then fixed and stained with 0.1% crystal violet solution (0.1% crystal violet, 20% methanol, 80% water) for 2H at RT. Then, crystal violet-stained cells were rinsed with PBS and water, plate was allowed to air-dry overnight. For imaging, whole-well images of the plate were scanned on the EVOS M7000 and percent area covered by crystal violet-stained cells was quantified using FIJI and analyzed using student's t-test.

Mouse Strains

NOD.Cg-Rag1^{tm1Mom} *Il2rg*^{tm1Wjl}*/SzJ* (NRG) mice were obtained from Dr. Jason Hanna (Purdue University) and used for allograft studies with murine iKRAS #3 cell lines (Collins et al.*J Clin,* 2012). *PDX1-Cre; LSL-Kras*^{G12D} (KC) and *PDX1-Cre; LSL-Kras*^{G12D}*; B56*$^{hm/hm}$ (KCB$^{hm/hm}$), *B56*$^{hm/hm}$*, and WT* genetically modified mice were composed of a 129S1/SvlmJ and C57/BL6 strain mixed background (129J/Bl6) and bred by S.Tinsley. These mice were used to identify acceleration of PDAC progression at 1MO, 2MO, and 5MO timepoints to identify healthy acinar area, number of PanINs/Area, and immunofluorescent staining of pancreatic tissues. These mice were also used for pancreatic explant cultures to test the ability of the cells to undergo acinar to ductal metaplasia (ADM) and to identify abrogation of ADM using DT061. Mouse genotypes were confirmed by clipping ears and utilizing the HOTSHOT DNA isolation protocol (Truett et al. *BioTechniques*, 2000) to extract DNA and utilized the primers in the table below. The PCR procedure was as follows: 95°C 2min, (95°C 30 sec, 60°C 30 sec, 72°C 40 sec) x 34 cycles, 72°C 5min, and HOLD at 4°C.

Fwd1-mB56a WT	*Mouse*	5'-CATCTggTTAgTCTTgAgATgC-3'
Fwd2-mB56a Mut	*Mouse*	5'-TATCCTgTTTggCCCATATTCAgC-3'
Rev-mB56a	*Mouse*	3'-ACTCTCAACACggTggTATCAAgg-5'
Fwd1-KRAS WT	*Mouse*	5'-ATgTCTTTCCCCAgCACAgT-3'

Fwd2-KRAS Mut	*Mouse*	5'-CTAgCCACCATggCTTgAgT-3'
Rev1-KRAS	*Mouse*	3'-TCCgAATTCAgTgACTACAgATg-5'
Fwd1-Cre positive	*Mouse*	5'-ACCAgCCAgCTATCAACTCg-3'
Fwd2-Cre control	*Mouse*	5'-CTAggCCACAgAATTgAAAgATCT-3'
Rev1-Cre positive	*Mouse*	3'-TTACATTggTCCAgCCACC-5'
Rev2-Cre control	*Mouse*	3'-gTAggTggAAATTCTAgCATCATCC-5'

Allograft Studies

iKRAS #3 stable cell lines (EV, B56αOE) were treated, counted, and resuspended in serum-free RPMI. Surgical sites of mice were shaved and treated with Nair to remove hair. The mice were then treated with 2mg/mL meloxicam and anesthetized with 2-3% isoflurane supplemented with 1g/L oxygen. Eyes were covered with ointment and surgical site was cleaned three times alternating with iodine and ethanol. Spleen location was identified, and incision was made just below the ribcage on the left side. Spleen was removed from abdomen with the pancreas following. Cells in RPMI was mixed 1:1 with Matrigel and 50uL of the cell mixture was injected into the pancreas. Mixture contained 5,000 cells per injection. Spleen and pancreas were returned into the abdomen and muscle layer was closed with two stitches and skin was closed using stables. Mice were monitored for recovery to sternal recumbency. Staples were removed after one week. Tumors were measured using the VEVO3100 rodent ultrasound machine and measured using Vevolab software.

Acinar-to-ductal metaplasia assays

ADM Assay protocol was adapted from Martinez and Storz. *JoVE,* (2019). Briefly, the collagen matrix was prepared consisting of 3.5mg/mL type I rat tail collagen, 1X Waymouth Media, and 7.7mM NaOH. 500µL of collagen matrix was added to the bottom of each well in a 12 well plate. Primary mouse acinar cells were obtained from $KCB^{hm/hm}$, KC, $B56^{hm/hm}$, and WT mice of 129J/Bl6 background. Mice were euthanized at 4-6 weeks by isoflurane induction followed by cervical

dislocation and subsequent cardiac puncture to endure death. 2-3 Pancreata per genotype were collected on ice in HBSS + 1% Pen/Strep and 100ng/mL Soybean Trypsin Inhibitor (STI). Pancreata were processed into small pieces using scalpels and then placed into 2mg/mL Collagenase I supplemented with 100ng/mL STI. Pancreata were incubated in collagenase solution for 20-30mins until small acinar clusters of approximately 100µm or less were visible under the microscope. Pancreatic tissue was broken up by gentle 1mL pipetting. Acinar cells were then pelleted at 900xg for 2mins at 4°C, removed from collagenase and washed with a 5%FBS/1%PenStrep/HBSS solution three times. Cells were then resuspended and passed through a 100µM filter to remove debris. Acinar cells were layered slowly on top of a 30%FBS/HBSS solution and separated by slow centrifugation at 200xg for 2mins at 4°C. FBS/HBSS solution was removed, and cells were resuspended and diluted in ADM Assay Media (1X Waymouth Media, 1% FBS, 100ng/mL STI, 1ng/mL Dexamethasone, and 1% Pen/Strep) until approximately 20 structures/10X field were observed in a 96 well plate. Acinar clusters in ADM assay media were mixed 1:1 with collagen matrix and 500µL of solution plated per well in a 12 well plate. Plate incubated at 37°C until collagen matrix solidified, and wells were topped with 500µL of ADM Assay Media. For ADM Assays testing DT061 efficacy in ADM, only KC genetic mice were used, and media was supplemented with DMSO or increasing doses of DT061. The acinar to ductal transdifferentiation process was observed using an EVOSM7000 through timelapse imaging every 3 hours for 72 hours total in an on-stage incubator maintaining 5% CO_2 and 37°C. 100 acinar structures per well, 3-4 wells/condition were followed throughout the 72H timelapse images and marked when transdifferentiated into duct-like structures using FIJI.

Tissue Immunofluorescence

Tissue slides were baked at 55°C for overnight and cooled to room temperature before proceeding. Slides incubated twice in xylene for 10 minutes and then rehydrated by incubation in 100% EtOH I, 100% EtOH II, 95% EtOH, 70% EtOH, and 100% PBS for 5 minutes each.

Slides were then cooked in a pressure cooker at high pressure for 10 minutes submerged in 1X High pH Antigen Retrieval Solution first (10 mM Tris, 1 mM EDTA solution), cooled to RT for 30min, rinsed in PBS, then cooked in the pressure cooker for an additional for 10mins in 1X Low pH Antigen Retrieval (pH 9.0, Low pH: 10mM Sodium Citrate, pH 6.0). Slides were cooled to room temperature for 30 minutes, then rinsed with PBS 3 times for 3 minutes each, and then a PAP pen was used to designate staining area on the slides. Slides were blocked in 3% BSA at room temperature for 1 hour. The blocking solution was blotted off and primary antibodies were diluted in 3% BSA with mouse-on-mouse kit (Vector Laboratories, #MKB-2213-1), and incubated at 4°C overnight. PBS-Tween (0.025%) was used to wash slides 3 times for 5 minutes each. Secondary antibody diluted to 1:200 in 3% BSA, incubated in the dark for 1 hour at room temperature. After secondary incubation, the slides were washed with PBS-Tween (0.025%) 3 times for 5 minutes each. Slides were incubated with DAPI at 1:1000 (Sigma-Aldrich #D9542) for 5 minutes, the excess solution was blotted off and coverslip was mounted using Prolong Gold Antifade Mountant (Invitrogen #P36934) and tissue was imaged on Nikon Eclipse N_i upright microscope and analyzed using FIJI.

KIAA1524	HPA039570	000008181	Atlas Biosciences
pS62 Myc	4B12	N/A	Rosalie Sears Lab
Amylase	A8273-1VL	0000121533	MilliporeSigma
Anti-pan Cytokeratin	sc-8108	J0721	Santa Cruz Biotechnologies
Chicken anti-Rat IgG (H+L), Alexa Fluor 488	A21470	2331905	Invitrogen
Goat anti-Mouse IgG (H+L), Alexa Fluor 647	A21235	UK290265	Invitrogen

Immunocytochemistry

Cells were fixed using 4% paraformaldehyde for 15 minutes at RT, washed with PBS 3 times for 5 minutes, then permeabilized using 0.3% triton-x100 for 25 minutes at RT. Cells were then stained using primary antibody diluted in 3% BSA and incubate overnight at 4°C. Cells were washed in PBST (0.025%) 3 times for 5 minutes and then stained with secondary antibody diluted in 3% BSA in the dark for one hour at RT. Cells were washed 3 times in PBST for 5 minutes. Cells were incubated with DAPI at 1:1000 (Sigma-Aldrich #D9542) for 5 minutes, the excess solution was blotted off and 12-50uL, or one drop, of Prolong Gold Antifade Mountant (Invitrogen #P36934) was added before coverslips were applied. Slides were allowed to harden and clarify overnight in the dark and sealed with clear nail polish before imaging. Cells were imaged on Nikon Eclipse N_i upright microscope and analyzed using FIJI.

KIAA1524	HPA039570	000008181	Atlas Biosciences
Goat anti-Rabbit IgG (H+L), Alexa Fluor 594	A32740	WK333741	Invitrogen

Alcian Blue Staining

The Alcian Blue (pH 2.5) Stain Kit (Vector Laboratories #H-3501) was used for this protocol. Tissue slides were baked at 62°C for 20 minutes and cooled to room temperature before proceeding. Slides were hydrated to distilled water; incubated in 100% xylene twice for 10 minutes, 100% EtOH twice for 5 minutes, 95% EtOH for 5 minutes, 70% EtOH for 5 minutes, and ddH2O twice for 5 minutes**.** Acetic Acid Solution was applied onto the tissue sections for 3 minutes, then the excess was tipped off. The Alcian Blue Solution was then applied to the tissue sections for 1 hour at 37°C. The slides were rinsed for 10-30 seconds in the Acetic Acid solution to remove the excess Alcian Blue Solution. The slides were rinsed for 2 minutes in running tap water followed by 2 changes of distilled water for 2 minutes each. Nuclear Fast Red solution was applied for 5 minutes. The slides were again rinsed for 2 minutes in running tap water

followed by 2 changes of distilled water for 2 minutes each. Slides were dehydrated through graded ethanol; incubated in ddH2O twice for 5 minutes, 70% EtOH for 5 minutes, 95% EtOH for 5 minutes, 100% EtOH twice for 5 minutes, and 100% xylene twice for 10 minutes. Mounting solution and coverslips were applied and sealed with clear nail polish. Images were taken at 10x magnification and tiled together using an EVOSM7000 to calculate the number of PanINs in the total pancreas tissue area. The number of alcian blue positive panINs were counted using FIJI and normalized by dividing the total area of the pancreatic tissue section stained.

Microtomy and IHC Tissue Staining

Tissue sections were taken at a thickness of 4 micrometers using a Thermo HM355S microtome. Sections were mounted on charged slides and dried for 30-60min in a 60C oven. For deparaffinization, slides were passed through two different Xylene incubations for 2mins each, two 100% ethanol incubations for 2mins each, then 1min through graded alcohols. Tissue was stained with Hematoxylin 7211 (Thermo Fisher #7211) for 2 minutes then incubated in an ammonia-based bluing solution for 1 min. Slides were rinsed and then dehydrated to 95% ethanol. Then Slides were incubated in an Eosin Y counter stain (Fisher #22-500-063) for 15 seconds. Slides were then dehydrated up to Xylene and allowed to dry at RT until Xylene was evaporated. Slides were cover slipped with Permount (Fisher #SP15-100) solution and sealed with clear nail polish. For the Masson's Trichrome Stain, the protocol outlined in "Carson, Freida L., and Christa Hladik Cappellano. Histotechnology: A Self-Instructional Text. 4th edition. Chicago: ASCP, 2015", was followed. The author(s) acknowledge the assistance of Victor Bernal-Crespo and the Purdue University Histology Research Laboratory, a core facility of the NIH-funded Indiana Clinical and Translational Science Institute.

RNA-Seq processing and Analysis

RNA was isolated using the ThermoScientific GeneJET Purification Kit (Thermofisher, #K0732). Eluted RNA concentration was measured using the Synergy H1. RNA was sent to Novogene for sequencing and resulting library and reads were analyzed by H. Kothandaraman and N.

Lanman at the Cancer Center Core for Bioinformatics at Purdue University to identify differentially regulated genes.

FIGURE LEGENDS

Figure 1: Oncogenic KRAS signaling promotes suppression of the PP2A-B56a complex. (A) Representative western of a timecourse of human pancreatic ductal epithelial (HPDE) cells with tet-inducible $KRAS^{G12D}$ (HPDE-iKRAS) treated with 50ng/mL doxycycline for 0-12H. **(B-D)** Quantification of CIP2A, Myc, and pERK/tERK protein expression at 0, 8, 12H $KRAS^{G12D}$ induction in HPDE-iKRAS cells. **(E)** Quantification of average puncta per cell of PLA between B56α and PP2Ac with 0H (OFF) or 8H (ON) of KRASG12D induction and treated with siNT siRNA or siRNA to CIP2A. Quantification is from one representative of three independent biological replicates. **(F)** Representative images of PLA quantified in E. Scale bars represent 20μM. **(G)** Representative images of three independent biological replicate stains of WT, 1MO, 2MO, and 5MO KC pancreatic tissue (left to right). IF stains indicate PanCk, Cip2a, pS62Myc, and MERGE of all stains (top to bottom). Scale bar represents 100μM. All experiments were repeated as three independent biological replicates and statistical analysis was performed using one-way ANOVA.

Figure 2: Loss of oncogenic KRAS signaling promotes activation of PP2A-B56a. (A) Representative western blot of loss of tet-inducible $KRAS^{G12D}$ signaling at 0-72 hours in iKRAS 3 cells. **(B)** Quantification of three independent replicates of western blot represented in A at 0H and 72H without $KRAS^{G12D}$ signaling. **(C)** Matching mRNA isolated from iKRAS 3 cells with loss of $KRAS^{G12D}$ signaling for 72 hours. Quantification includes three independent biological replicates. **(E)** Representative images of pancreatic tissue from iKRAS* mouse models after 3W of dox-induced $KRAS^{G12D}$ signaling (top) or after 1W of dox withdrawal (bottom). Immunofluorescent staining of PanCk, Cip2a, pS62Myc, and all stains merged (left to right). Statistical analysis was performed using one-way ANOVA. All data representative of 3-4 biological replicates.

Figure 3: Overexpression of B56a abrogates oncogenic phenotypes. (A) Soft agar assay of stable iKRAS 3 cell line with empty vector control or overexpression of B56α, stained with crystal violet and scanned after two weeks of growth. **(B)** Quantification of four biological replicates of the soft agar assay represented as fold change relative to the number of colonies formed in the iKRAS 3 empty vector control. **(C)** Clonogenic assay of iKRAS 3 cells with empty vector control or overexpression of B56α stained with crystal violet after six days. **(D)** Quantification of three replicates of clonogenic assay, measured by fold change in the percent area covered by cells. Quantified on FIJI. **(E)** Endpoint tumor weight in grams of each condition. EV n = 8, B56α OE n = 9). **(F)** Growth curve of an orthotopic pancreatic allograft of iKRAS 3 EV or B56αOE cell lines in NRG mice, measured by volume of tumor in mm^3. **(G)** Picture of orthotopic tumors at endpoint displayed from largest (right) to smallest (left) in each condition (top: EV,

bottom: B56αOE). **(H)** Representative images of immunofluorescent staining from EV (top) or B56αOE (bottom) tumors. Stains in images represent PanCk, HA-tag, pS62 Myc, and merged images (left to right). All experiments performed at least three times independently and statistical analysis was done using student's t-test.

Figure 4: Loss of B56a promotes acceleration of acinar to ductal metaplasia. (A) Representative images of acinar cells isolated form WT, B56a$^{hm/hm}$, KC, and KCB$^{hm/hm}$ genetic mouse models cultured in collagen for 24, 48, and 72 hours. **(C)** Overall percent of ductal-like structures present in collagen in each condition at 24, 48, and 72 hours post-collagen implantation, representative of five independent biological replicates. **(C)** Timecourse of acinar to ductal transdifferentiation kinetics of each condition over three days, quantified every 6 hours. Timecourse includes data from one representative biological replicate. **(D)** mRNA expression of ductal cell marker, *ck19*, in each genotype at 24, 48, and 72H timepoints. **(E)** Differentially expressed genes in RNA-seq of KC and KCB$^{hm/hm}$ structures at the 48H timepoint at FDR = 0.05. **(F-G)** Gene set enrichment analysis of ranked DEGs upregulated in KCB$^{hm/hm}$ compared to KC control. Statistical analysis performed using either a t-test of the area under the curve or one-way ANOVA.

Figure 5: Loss of B56a promotes progression of PDAC precursor lesions. (A) Representative 2MO or 5MO timepoints from pancreatic tissue in respective genetic mouse models stained with H&E (top), Massons Trichrome (middle), and alcian blue (bottom). **(B-D)** Quantifications of healthy acinar area, stromal content, and number of PanINs quantified from stains represented in A, respectively, at 2MO and 5MO timepoints. All analysis represented at least 6 biological replicates per condition. **(E)** Amylase, Cip2a, pS62Myc, and merged immunofluorescent stains in pancreata harvested 2MO KC or KCB$^{hm/hm}$ mice. **(F)** PanCk, Cip2a, pS62 Myc and merged immunofluorescent stains in pancreata harvested 2MO KC or KCB$^{hm/hm}$ mice. All images representative of at least three independent biological replicates.

Figure 6: Re-activation of PP2A-B56a prevents initiation of pancreatic cancer. (A) Representative images of acinar to ductal differentiation in KC acinar cells after 72H in collagen and treated with increasing doses of SMAP, DT061. **(B)** Percent duct-like structures over total structures present at each concentration of DT061 treatment. **(C)** Average ductal lumen size of duct-like structures in each condition. **(D)** Distribution of the ductal lumen measurements at each concentration of DT061. **(E-H)** qPCR of mRNA isolated from the organoids in collagen after 72H of DT061 treatment at each concentration dosed. **(J)** Survival curve of *PDX1-Cre; P53$^{+/-}$; LSL-KRAS^{G12D}* (KPC) Mice enrolled in a survival experiment treated twice daily with 15mg/kg DT061 via oral gavage or with vehicle until mice succumb to PDAC disease burden.

SUPPLEMENTAL FIGURE LEGENDS

Supplemental 1. (A) Disease-free survival of patients stratified by expression of *B56a* mRNA. Graph generated from publicly available data on CBioPortal. **(B)** Representative immunofluorescent images of CIP2A expression from siCIP2A KD in PLA experiment. **(C)** Representative images of clonogenic assay performed with HPDE-iKRAS cells with either siNT or siCIP2A treatment. **(D)** Quantification of three independent replicates of

clonogenic assay represented in C. Statistical analysis performed using student's t-test or one-way ANOVA.

Supplement Figure 2. (A) Percent of total structures that appear duct-like after 24, 48, and 72H in collagen. Replicates represent three independent replicates that were used for RNA-seq omics analysis. **(B-D)** mRNA expression of *sox9*, *myc,* and *cip2a* (top to bottom) in each genotype at 24, 48, and 72H timepoints

Supplemental 3. (A) Amylase, Cip2a, pS62Myc, and merged immunofluorescent stains in pancreata harvested 5MO KC or $KCB^{hm/hm}$ mice. **(B)** PanCk, Cip2a, pS62 Myc and merged immunofluorescent stains in pancreata harvested 5MO KC or $KCB^{hm/hm}$ mice. All images representative of at least three independent biological replicates.

REFERENCES

1. Hobbs GA, Der CJ, Rossman KL. RAS isoforms and mutations in cancer at a glance. J Cell Sci. 2016;129:1287–92.

2. Siegel RL, Miller KD, Wagle NS, Jemal A. Cancer statistics, 2023. Ca Cancer J Clin. 2023;73:17–48.

3. Bryant KL, Mancias JD, Kimmelman AC, Der CJ. KRAS: feeding pancreatic cancer proliferation. Trends Biochem Sci. 2014;39:91–100.

4. Hingorani SR, Petricoin EF, Maitra A, Rajapakse V, King C, Jacobetz MA, et al. Preinvasive and invasive ductal pancreatic cancer and its early detection in the mouse. Cancer Cell. 2003;4.

5. Collins MA, Bednar F, Zhang Y, Brisset J-C, Galbán S, Galbán CJ, et al. Oncogenic Kras is required for both the initiation and maintenance of pancreatic cancer in mice. J Clin Invest. 2012;122:639–53.

6. Storz P. Acinar cell plasticity and development of pancreatic ductal adenocarcinoma. Nat Rev Gastroentero. 2017;14:296–304.

7. Collado M, Gil J, Efeyan A, Guerra C, Schuhmacher AJ, Barradas M, et al. Senescence in premalignant tumours. Nature. 2005;436:642–642.

8. Sablina AA, Hector M, Colpaert N, Hahn WC. Identification of PP2A Complexes and Pathways Involved in Cell Transformation. Cancer Res. 2010;70:10474–84.

9. Sangodkar J, Farrington CC, McClinch K, Galsky MD, Kastrinsky DB, Narla G. All roads lead to PP2A: exploiting the therapeutic potential of this phosphatase. Febs J. 2016;283:1004–24.

10. Hydbring P, Larsson L-G. Cdk2: a key regulator of the senescence control function of Myc. Aging Albany NY. 2010;2:244–50.

11. Karnoub AE, Weinberg RA. Ras oncogenes: split personalities. Nat Rev Mol Cell Biology. 2008;9:517–31.

12. Letourneux C, Rocher G, Porteu F. B56-containing PP2A dephosphorylate ERK and their activity is controlled by the early gene IEX-1 and ERK. Embo J. 2006;25:727–38.

13. Lin SS, Bassik MC, Suh H, Nishino M, Arroyo JD, Hahn WC, et al. PP2A Regulates BCL-2 Phosphorylation and Proteasome-mediated Degradation at the Endoplasmic Reticulum*. J Biol Chem. 2006;281:23003–12.

14. Farrell AS, Allen-Petersen B, Daniel CJ, Wang X, Wang Z, Rodriguez S, et al. Targeting Inhibitors of the Tumor Suppressor PP2A for the Treatment of Pancreatic Cancer. Mol Cancer Res. 2014;12:924–39.

15. Janghorban M, Langer EM, Wang X, Zachman D, Daniel CJ, Hooper J, et al. The tumor suppressor phosphatase PP2A-B56α regulates stemness and promotes the initiation of malignancies in a novel murine model. Plos One. 2017;12:e0188910.

16. Kauko O, Laajala TD, Jumppanen M, Hintsanen P, Suni V, Haapaniemi P, et al. Label-free quantitative phosphoproteomics with novel pairwise abundance normalization reveals synergistic RAS and CIP2A signaling. Sci Rep-uk. 2015;5:13099.

17. Chang W-H, Liu Y, Hammes EA, Bryant KL, Cerione RA, Antonyak MA. Oncogenic RAS promotes MYC protein stability by upregulating the expression of the inhibitor of apoptosis protein family member Survivin. J Biological Chem. 2023;299:102842.

18. Wu Y, Gu T-T, Zheng P-S. CIP2A cooperates with H-Ras to promote epithelial–mesenchymal transition in cervical-cancer progression. Cancer Lett. 2015;356:646–55.

19. Arnold HK, Sears RC. Protein Phosphatase 2A Regulatory Subunit B56α Associates with c-Myc and Negatively Regulates c-Myc Accumulation†. Mol Cell Biol. 2006;26:2832–44.

20. Farrell AS, Sears RC. MYC Degradation. Csh Perspect Med. 2014;4:a014365.

21. Sears R, Leone G, DeGregori J, Nevins JR. Ras Enhances Myc Protein Stability. Mol Cell. 1999;3:169–79.

22. Seeling JM, Miller JR, Gil R, Moon RT, White R, Virshup DM. Regulation of β-Catenin Signaling by the B56 Subunit of Protein Phosphatase 2A. Science. 1999;283:2089–91.

23. Martinez AKF, Storz P. Mimicking and Manipulating Pancreatic Acinar-to-Ductal Metaplasia in 3-dimensional Cell Culture. J Vis Exp. 2019;

24. Sodir NM, Kortlever RM, Barthet VJA, Campos T, Pellegrinet L, Kupczak S, et al. Myc instructs and maintains pancreatic adenocarcinoma phenotype. Cancer Discov. 2020;CD-19-0435.

25. Thomas D, Radhakrishnan P. Tumor-stromal crosstalk in pancreatic cancer and tissue fibrosis. Molecular Cancer. 2019;18.

26. Leonard D, Huang W, Izadmehr S, O'Connor CM, Wiredja DD, Wang Z, et al. Selective PP2A Enhancement through Biased Heterotrimer Stabilization. Cell. 2020;

27. Kemp SB, Cheng N, Markosyan N, Sor R, Kim I-K, Hallin J, et al. Efficacy of a small molecule inhibitor of KrasG12D in immunocompetent models of pancreatic cancer. Cancer Discov. 2022;13:298–311.

28. Hosein AN, Dougan SK, Aguirre AJ, Maitra A. Translational advances in pancreatic ductal adenocarcinoma therapy. Nat Cancer. 2022;3:272–86.

29. Chen B, Hu H, Chen X. From Basic Science to Clinical Practice: The Role of Cancerous Inhibitor of Protein Phosphatase 2A (CIP2A)/p90 in Cancer. Frontiers Genet. 2023;14:1110656.

30. Khanna A, Okkeri J, Bilgen T, Tiirikka T, Vihinen M, Visakorpi T, et al. ETS1 Mediates MEK1/2-Dependent Overexpression of Cancerous Inhibitor of Protein Phosphatase 2A (CIP2A) in Human Cancer Cells. Plos One. 2011;6:e17979.

31. Aakula A, Sharma M, Tabaro F, Nätkin R, Kamila J, Honkanen H, et al. RAS and PP2A activities converge on epigenetic gene regulation. Life Sci Alliance. 2023;6:e202301928.

32. Sangodkar J, Perl A, Tohme R, Kiselar J, Kastrinsky DB, Zaware N, et al. Activation of tumor suppressor protein PP2A inhibits KRAS-driven tumor growth. J Clin Investigation. 2017;127:2081–90.

33. Tohmé R, Izadmehr S, Gandhe S, Tabaro G, Vallabhaneni S, Thomas A, et al. Direct activation of PP2A for the treatment of tyrosine kinase inhibitor–resistant lung adenocarcinoma. Jci Insight. 2019;4:e125693.

34. Kauko O, O'Connor CM, Kulesskiy E, Sangodkar J, Aakula A, Izadmehr S, et al. PP2A inhibition is a druggable MEK inhibitor resistance mechanism in KRAS-mutant lung cancer cells. Sci Transl Med. 2018;10:eaaq1093.

35. McClinch K, Avelar RA, Callejas D, Izadmehr S, Wiredja D, Perl A, et al. Small-Molecule Activators of Protein Phosphatase 2A for the Treatment of Castration-Resistant Prostate Cancer. Cancer Res. 2018;78:2065–80.

36. Avelar RA, Armstrong AJ, Carvette G, Gupta R, Puleo N, Colina JA, et al. Small molecule mediated stabilization of PP2A modulates the Homologous Recombination pathway and potentiates DNA damage-induced cell death. Mol Cancer Ther. 2023;22:599–615.

37. Allen-Petersen BL, Risom T, Feng Z, Wang Z, Jenny ZP, Thoma MC, et al. Activation of PP2A and inhibition of mTOR synergistically reduce MYC signaling and decrease tumor growth in pancreatic ductal adenocarcinoma. Cancer Res. 2018;79:209–19.

Figure 1

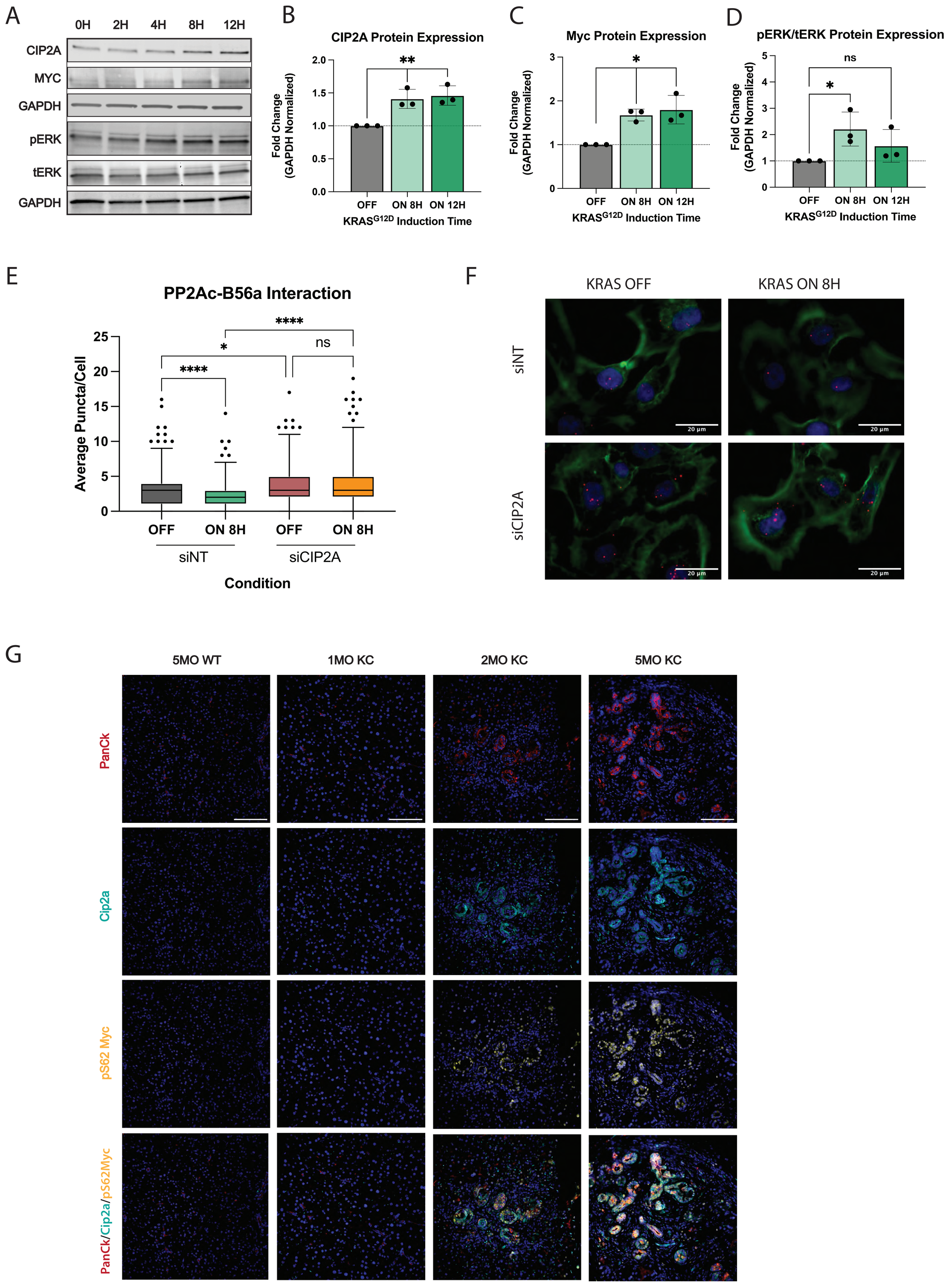
A
0H
2H
4H
8H
12H
CIP2A
MYC
GAPDH
pERK
tERK
GAPDH
B
CIP2A Protein Expression
Fold Change (GAPDH Normalized)
OFF
ON 8H
ON 12H
KRAS^{G12D} Induction Time
C
Myc Protein Expression
Fold Change (GAPDH Normalized)
OFF
ON 8H
ON 12H
KRAS^{G12D} Induction Time
D
pERK/tERK Protein Expression
Fold Change (GAPDH Normalized)
ns
OFF
ON 8H
ON 12H
KRAS^{G12D} Induction Time
E
PP2Ac-B56a Interaction
Average Puncta/Cell
****
ns
OFF
ON 8H
OFF
ON 8H
siNT
siCIP2A
Condition
F
KRAS OFF
KRAS ON 8H
siNT
siCIP2A
20 µm
G
5MO WT
1MO KC
2MO KC
5MO KC
PanCk
Cip2a
pS62 Myc
PanCk/Cip2a/pS62Myc

Figure 2

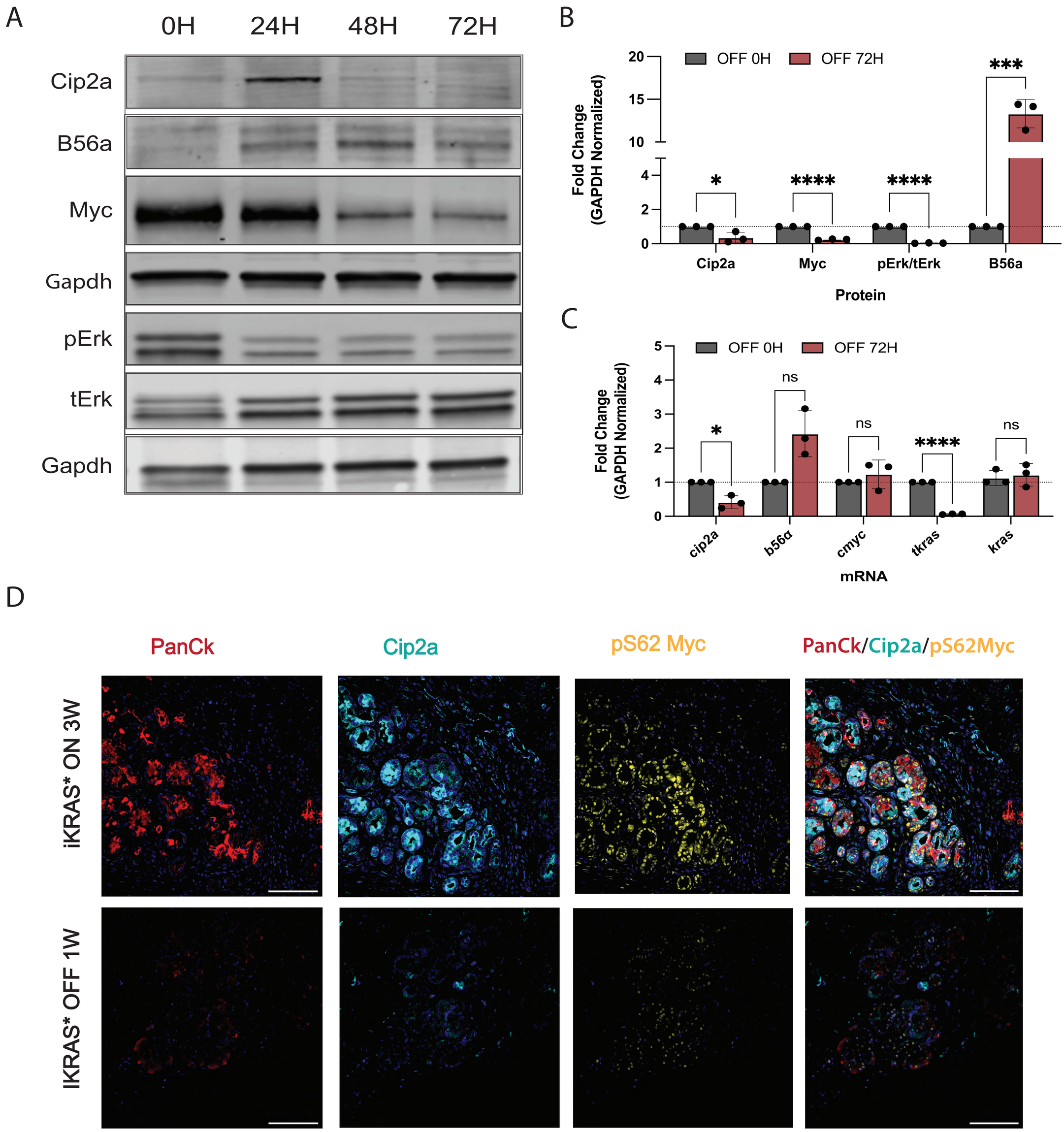
A
0H
24H
48H
72H
Cip2a
B56a
Myc
Gapdh
pErk
tErk
Gapdh
B
OFF 0H
OFF 72H
Fold Change (GAPDH Normalized)
20
15
10
4
2
0
*
****
****
***
Cip2a
Myc
pErk/tErk
B56a
Protein
C
OFF 0H
OFF 72H
Fold Change (GAPDH Normalized)
5
4
3
2
1
0
*
ns
ns
****
ns
cip2a
b56α
cmyc
tkras
kras
mRNA
D
PanCk
Cip2a
pS62 Myc
PanCk/Cip2a/pS62Myc
iKRAS* ON 3W
IKRAS* OFF 1W

Figure 3

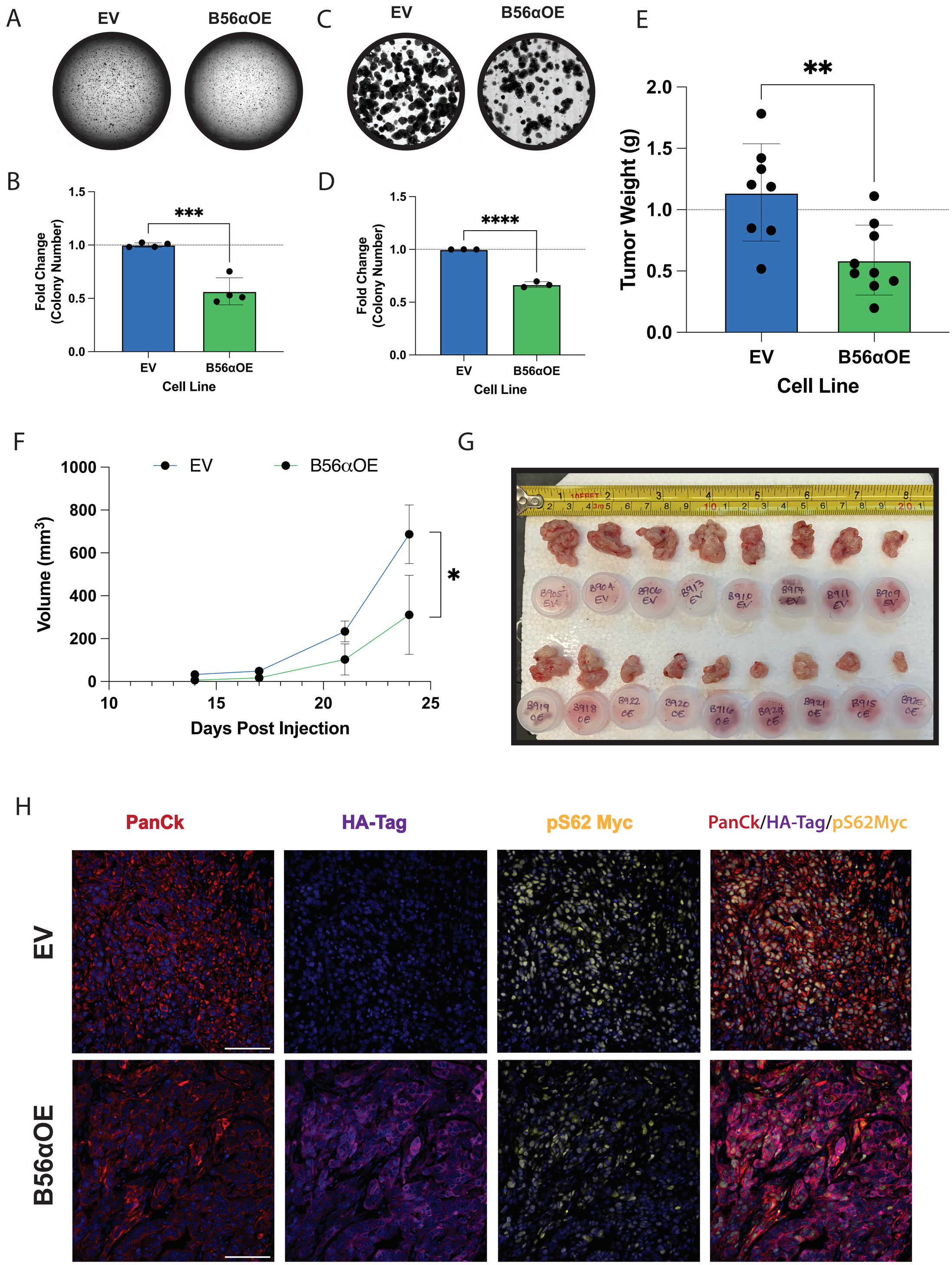
A
EV
B56αOE
C
EV
B56αOE
E
**
Tumor Weight (g)
2.0
1.5
1.0
0.5
0.0
EV
B56αOE
Cell Line
B
***
Fold Change (Colony Number)
1.5
1.0
0.5
0.0
EV
B56αOE
Cell Line
D
****
Fold Change (Colony Number)
1.5
1.0
0.5
0.0
EV
B56αOE
Cell Line
F
EV
B56αOE
Volume (mm³)
1000
800
600
400
200
0
10
15
20
25
Days Post Injection
*
G
H
PanCk
HA-Tag
pS62 Myc
PanCk/HA-Tag/pS62Myc
EV
B56αOE

Figure 4

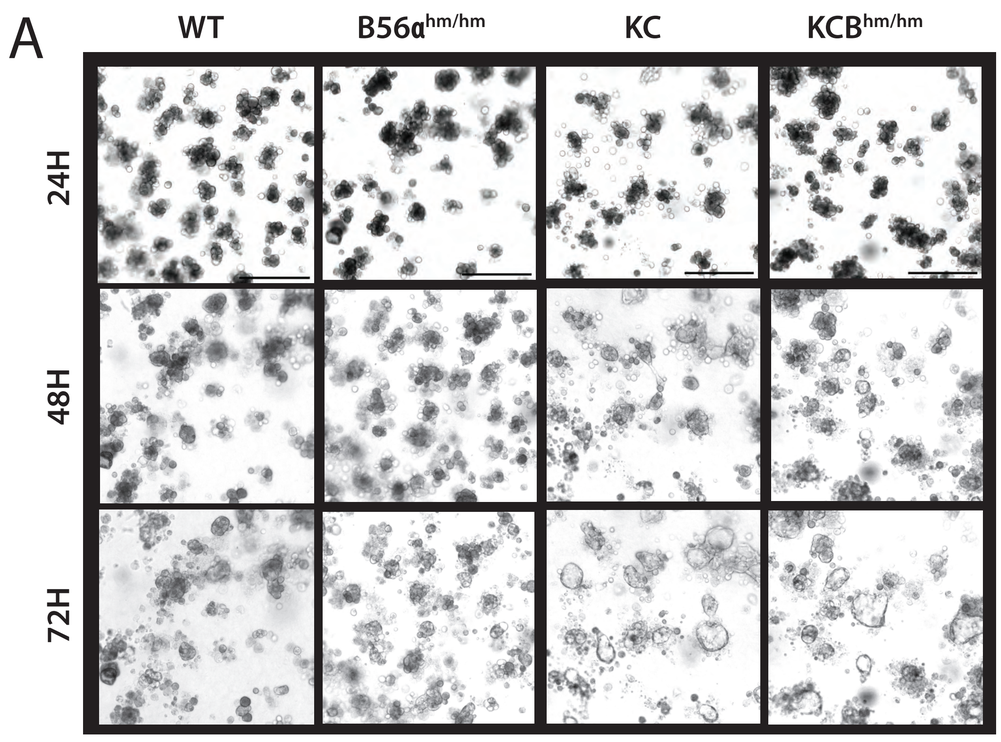
A
WT
B56α hm/hm
KC
KCB hm/hm
24H
48H
72H

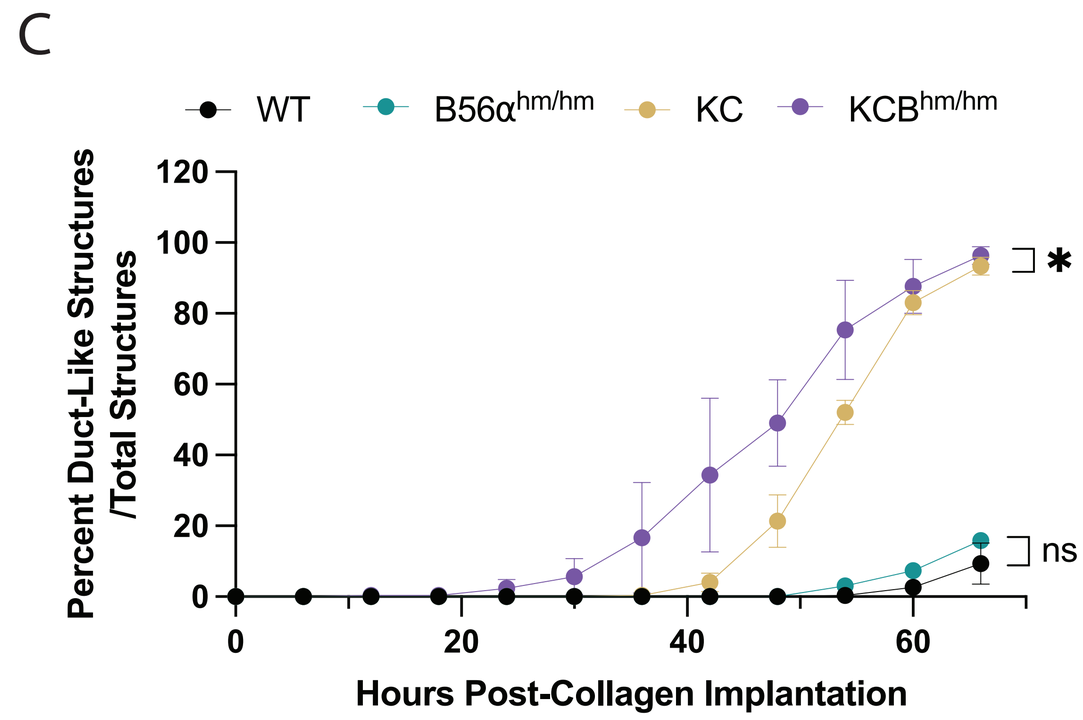
C
WT
B56α hm/hm
KC
KCB hm/hm
Percent Duct-Like Structures /Total Structures
Hours Post-Collagen Implantation
*
ns

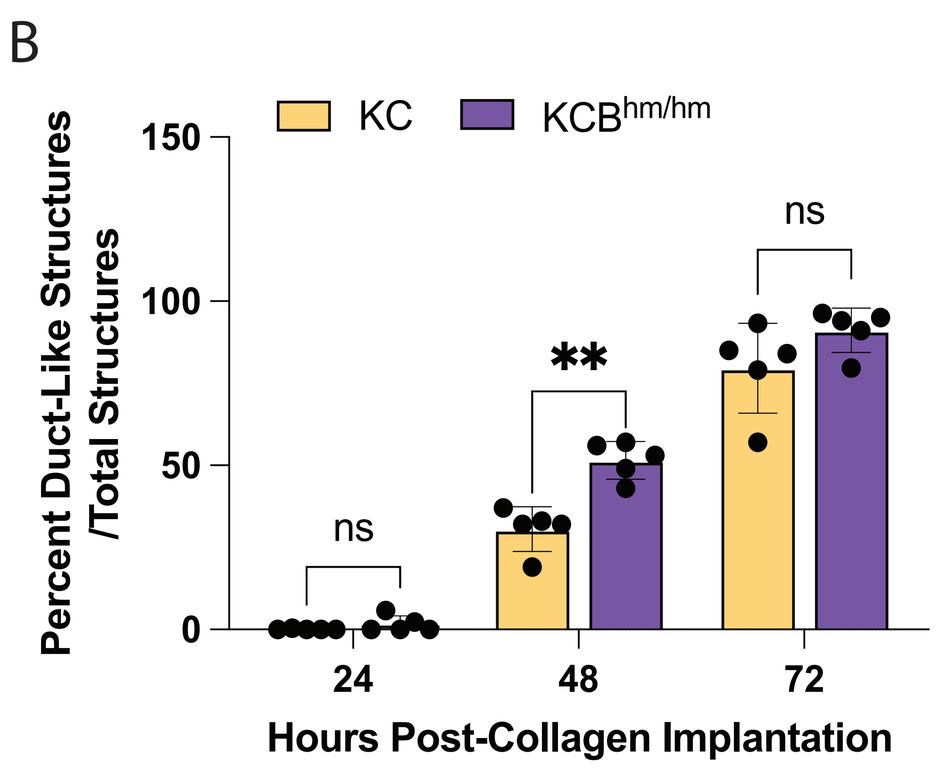
B
KC
KCB hm/hm
Percent Duct-Like Structures /Total Structures
Hours Post-Collagen Implantation
ns
**
ns

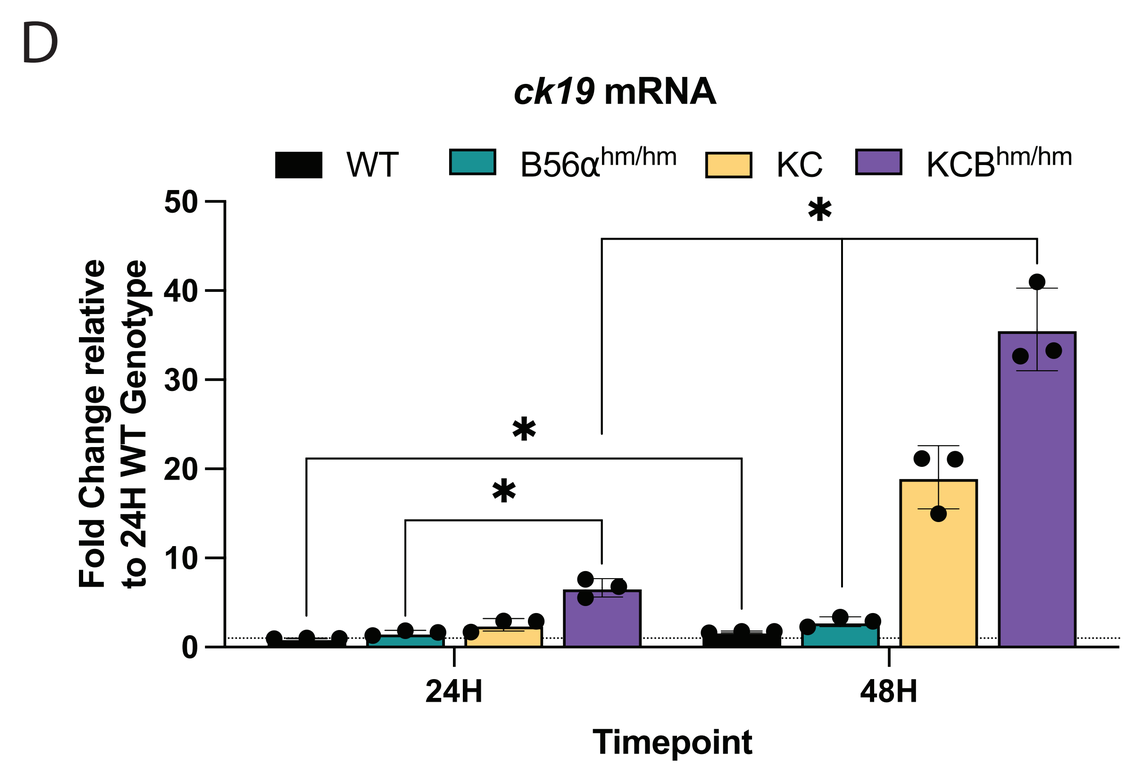
D
ck19 mRNA
WT
B56α hm/hm
KC
KCB hm/hm
Fold Change relative to 24H WT Genotype
Timepoint
24H
48H
*
*
*

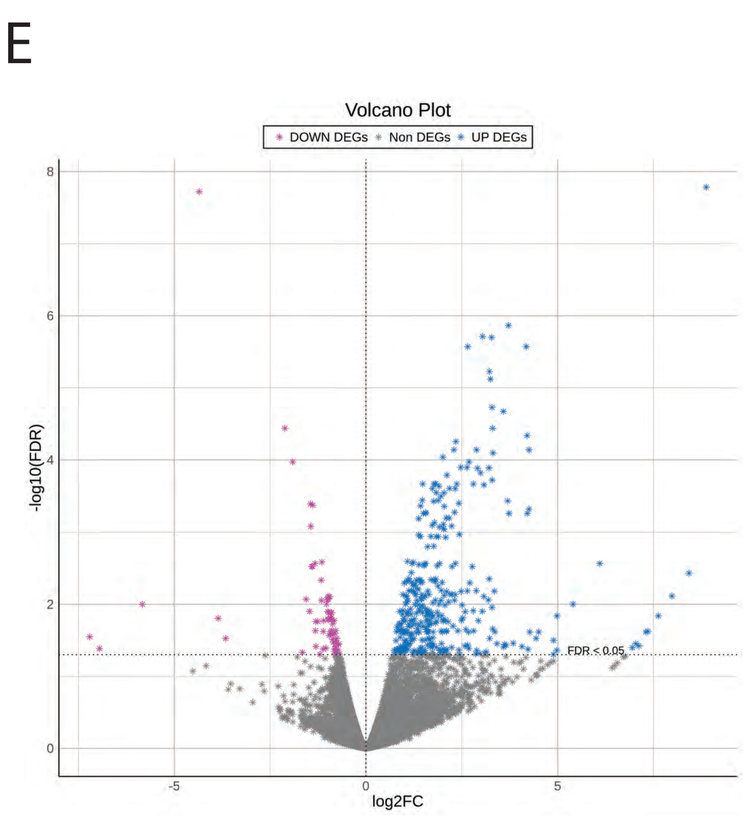
E
Volcano Plot
DOWN DEGs
Non DEGs
UP DEGs
-log10(FDR)
log2FC
FDR < 0.05

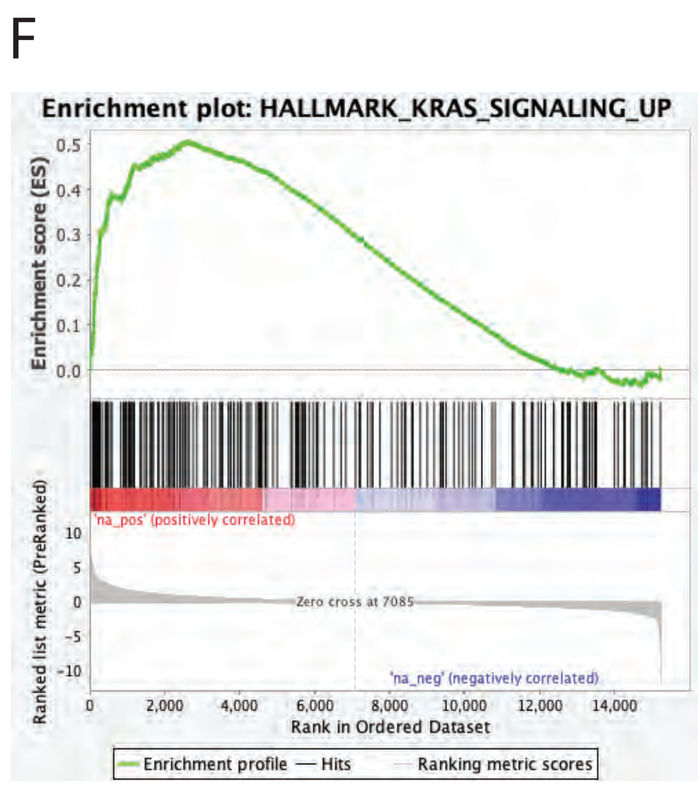
F
Enrichment plot: HALLMARK_KRAS_SIGNALING_UP
Enrichment score (ES)
Ranked list metric (PreRanked)
'na_pos' (positively correlated)
Zero cross at 7085
'na_neg' (negatively correlated)
Rank in Ordered Dataset
Enrichment profile
Hits
Ranking metric scores

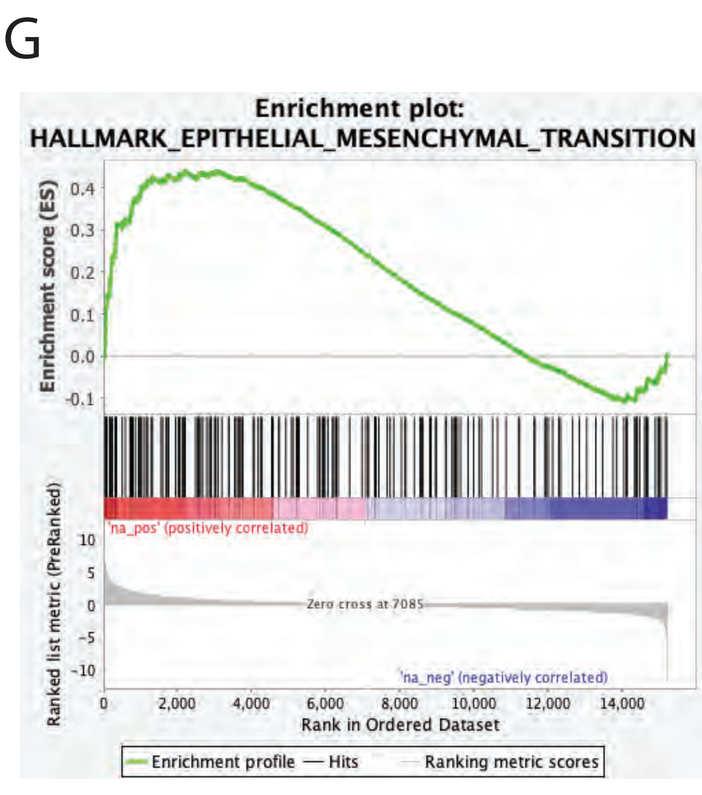
G
Enrichment plot: HALLMARK_EPITHELIAL_MESENCHYMAL_TRANSITION
Enrichment score (ES)
Ranked list metric (PreRanked)
'na_pos' (positively correlated)
Zero cross at 7085
'na_neg' (negatively correlated)
Rank in Ordered Dataset
Enrichment profile
Hits
Ranking metric scores

Figure 5

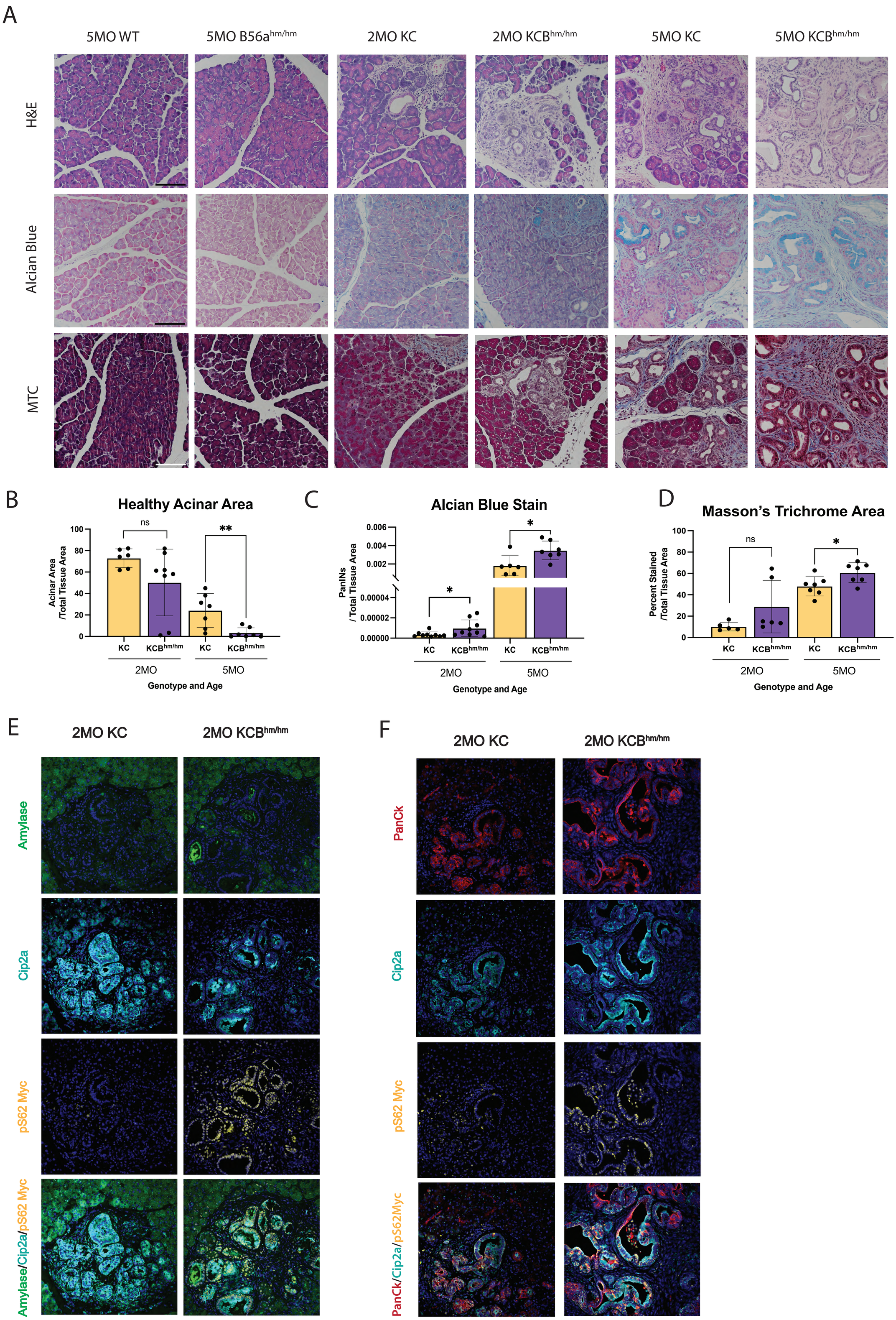
A
5MO WT
5MO B56a hm/hm
2MO KC
2MO KCB hm/hm
5MO KC
5MO KCB hm/hm
H&E
Alcian Blue
MTC
B
Healthy Acinar Area
Acinar Area /Total Tissue Area
ns
**
KC
KCB hm/hm
KC
KCB hm/hm
2MO
5MO
Genotype and Age
C
Alcian Blue Stain
PanINs / Total Tissue Area
*
*
KC
KCB hm/hm
KC
KCB hm/hm
2MO
5MO
Genotype and Age
D
Masson's Trichrome Area
Percent Stained /Total Tissue Area
ns
*
KC
KCB hm/hm
KC
KCB hm/hm
2MO
5MO
Genotype and Age
E
2MO KC
2MO KCB hm/hm
Amylase
Cip2a
pS62 Myc
Amylase/Cip2a/pS62 Myc
F
2MO KC
2MO KCB hm/hm
PanCk
Cip2a
pS62 Myc
PanCk/Cip2a/pS62Myc

Figure 6

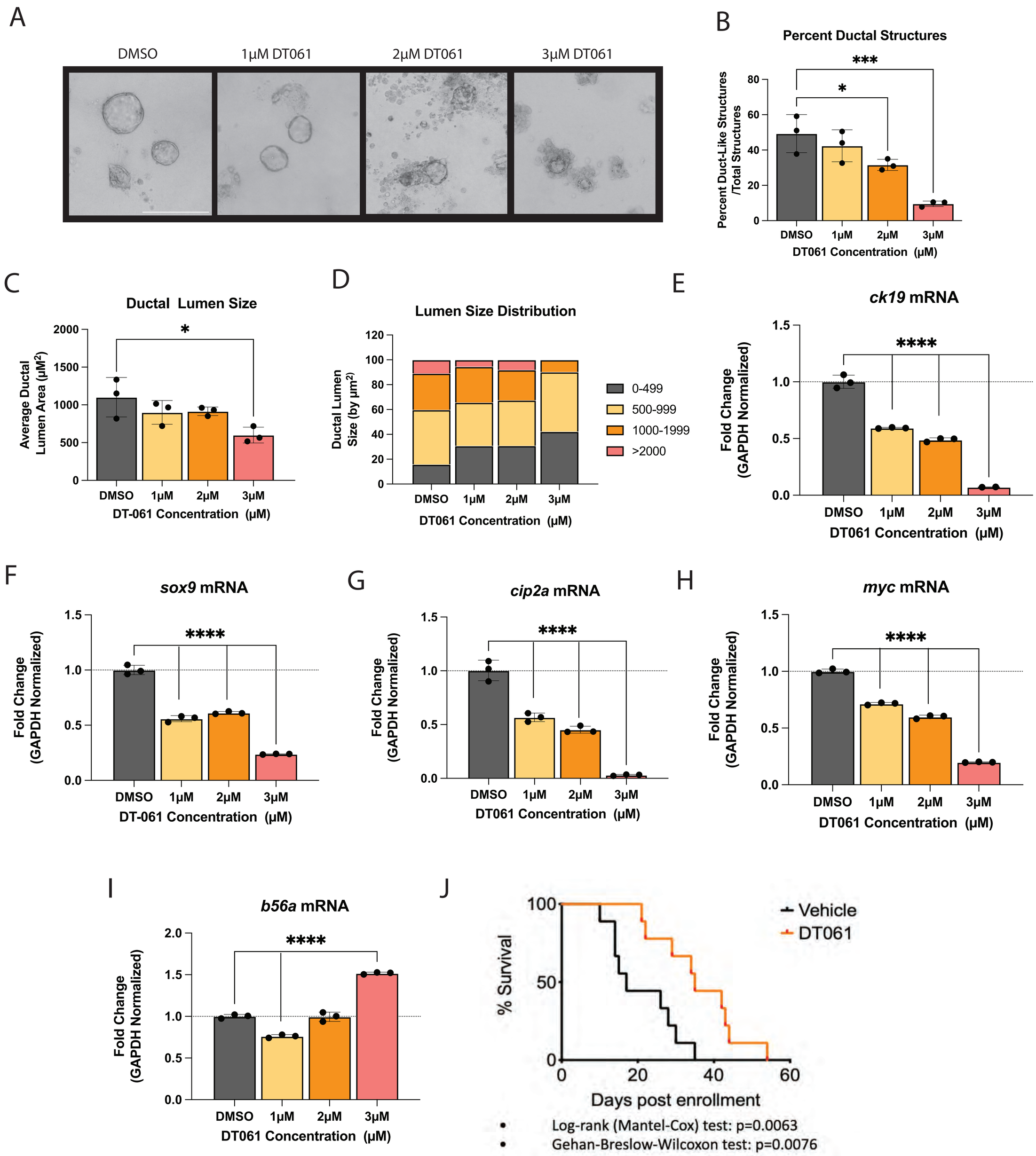
A
DMSO
1μM DT061
2μM DT061
3μM DT061
B
Percent Ductal Structures
Percent Duct-Like Structures /Total Structures
DMSO 1μM 2μM 3μM
DT061 Concentration (μM)
C
Ductal Lumen Size
Average Ductal Lumen Area (μM²)
DT-061 Concentration (μM)
D
Lumen Size Distribution
Ductal Lumen Size (by μm²)
0-499
500-999
1000-1999
>2000
DT061 Concentration (μM)
E
ck19 mRNA
Fold Change (GAPDH Normalized)
DT061 Concentration (μM)
F
sox9 mRNA
DT-061 Concentration (μM)
G
cip2a mRNA
DT061 Concentration (μM)
H
myc mRNA
DT061 Concentration (μM)
I
b56a mRNA
DT061 Concentration (μM)
J
Vehicle
DT061
% Survival
Days post enrollment
Log-rank (Mantel-Cox) test: p=0.0063
Gehan-Breslow-Wilcoxon test: p=0.0076